

Letters

EMI Suppression in Inductive Power Transfer Systems Using Class E Inverters

Heyuan Li ¹, Graduate Student Member, IEEE, Haoyu Wang ², Senior Member, IEEE,
Junrui Liang ³, Senior Member, IEEE, and Minfan Fu ⁴, Senior Member, IEEE

Abstract—The coupler’s antenna-like structure introduces electromagnetic interference (EMI) challenges in inductive power transfer systems. This letter leverages the spread spectrum technique in a class E inverter-driven, highly resonant system to address these challenges. However, a conventional class E inverter would be optimized toward a single frequency, and directly leading to hard switching issue when applying spread spectrum. By examining original classical class-E design method, it enriches the understanding of the design under frequency modulation scenarios. Through simulation, it investigates the tradeoffs among various goals, including efficiency, voltage stress, output ripple, and EMI reduction. It develops an IPT system according to the design strategy, achieving zero-voltage switching across a frequency modulation range of 0.95–1.05 MHz and maintaining an efficiency of 87%. This approach resulted in a 13-dB EMI reduction compared to a 1 MHz classical class E design.

Index Terms—Class E inverter, electromagnetic interference (EMI), frequency modulation, inductive power transfer (IPT), spread spectrum.

I. INTRODUCTION

INDUCTIVE power transfer (IPT) systems have been extensively deployed in a myriad of applications. Over recent years, much of the scholarly work has focused on the development of systems that are capable of catering to a breadth of requirements, including stable output, high efficiency, high misalignment tolerance, and enhanced stability. Presently, there is more emphasis on addressing concerns related to electromagnetic interference (EMI) emissions [1]. The antenna-like coupler introduces challenges associated with EMI, necessitating further investigation. Efforts to mitigate radiative EMI through coupler

design optimization [2], implementation of shielding [3], [4], and the use of metamaterials [5] have been developed.

The spread spectrum technique, referenced as [6], is extensively employed in power converters to mitigate EMI. It functions by spreading the energy over a broader frequency range rather than focusing it on a single frequency point. This is accomplished through the modulation of frequency. Integrating the spread spectrum method within a resonant converter requires careful attention to its intrinsic sensitivity to frequency variations. Deviations from the original resonance conditions may lead to considerable output fluctuations and augment switching losses as a result of zero-voltage switching (ZVS) failure. To address them, the introduction of supplementary components to form the resonant network is imperative, alongside the design of control strategies aimed at minimizing output ripple. The application of spread spectrum in IPT systems would use diverse automatic tuning circuits to maintain resonance amidst frequency modulation [7], [8], [9]. This adaptation generally requires additional sensors and enhancement of transmitter-receiver (TX-RX) communication capabilities, further complicating the system architecture.

This article introduces a novel approach to integrating spread spectrum techniques into highly resonant IPT systems that use single-switch inverters, a configuration typically found in high-frequency, low-power applications. Unlike bridge inverters, elements including the transistor, compensation network, and coupler contribute to the final resonance. This integration increases the system’s sensitivity, particularly when employing spread spectrum technique. A key innovation of this work is the use of the class E inverter as a case study to explore design strategies that achieve multiple performance objectives. By moving beyond traditional fixed-frequency design constraints, proposed method offers increased flexibility, particularly under frequency modulation. This study delves into the tradeoffs between crucial factors like system efficiency, switch voltage stress, output ripple, and EMI.

II. LOW-RADIATION DESIGN

A. Spread Spectrum in IPT

Fig. 1 elaborates on an IPT system driven by a class E inverter, featuring key elements, such as a transistor denoted as S , a choke inductor L_f , a shunt capacitor C_1 , compensation capacitors on

Received 2 July 2024; revised 12 August 2024; accepted 4 September 2024. Date of publication 10 September 2024; date of current version 7 October 2024. This work was supported by the National Natural Science Foundation of China under Grant 52477013. (Corresponding author: Minfan Fu.)

Heyuan Li is with the School of Information Science and Technology, ShanghaiTech University, Shanghai 201210, China, also with the Advanced Research Institute, Chinese Academy of Sciences, Shanghai 201210, China, also with the Shanghai Institute of Microsystem and Information Technology, Chinese Academy of Sciences, Shanghai 200050, China, and also with the University of Chinese Academy of Sciences, Beijing 100049, China.

Haoyu Wang, Junrui Liang, and Minfan Fu are with the School of Information Science and Technology, ShanghaiTech University, Shanghai 201210, China, and also with the Shanghai Engineering Research Center of Energy Efficient and Custom AI IC, Shanghai 201210, China (e-mail: fumf@shanghaitech.edu.cn).

Color versions of one or more figures in this article are available at <https://doi.org/10.1109/TPEL.2024.3457152>.

Digital Object Identifier 10.1109/TPEL.2024.3457152

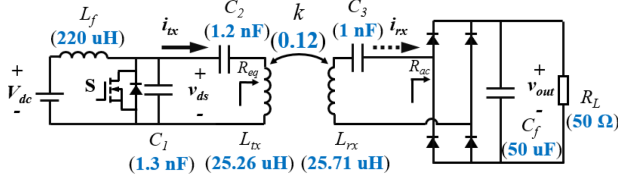


Fig. 1. Typical IPT system driven by a class E inverter.

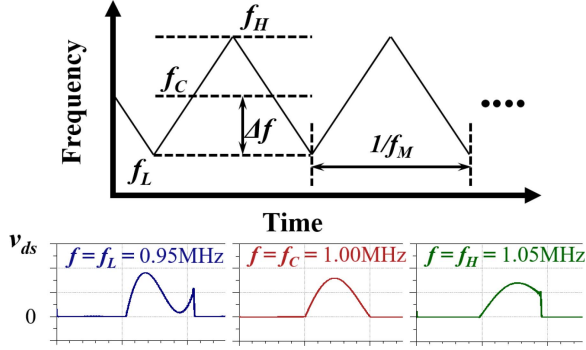


Fig. 2. Spread spectrum using triangular modulation.

the TX side (C_2) and the RX side (C_3), an inductive coupler, a bridge rectifier, and a load symbolized by R_L . This system is acclaimed for optimally harnessing the salient features of the class E inverter including zero voltage switching (ZVS) and zero-voltage derivative switching (ZVDS). The inductive coupler is modeled by two inductors L_{tx} and L_{rx} along with a coupling coefficient k . At a fixed switching frequency f_s , the capacitor C_3 is precisely tuned to resonate with L_{rx} , satisfying the condition $\omega_s L_{rx} - 1/(\omega_s C_3) = 0$. All the voltage and current are defined in Fig. 1. At TX side, an equivalent ac resistance, R_{eq} , represents the combined loading and coupling influences, which subsequently directs the configuration of C_1 and C_2 for a classical design [10]

$$\begin{cases} \omega_s C_1 = \frac{1}{\omega_s L_{tx} - \frac{\pi(\pi^2-4)R_{eq}}{16}} \\ \omega_s C_2 = \frac{8}{\pi(\pi^2+4)R_{eq}} \end{cases} \quad (1)$$

When the selection of C_1 and C_2 is freed from strict adherence to constraints linked to f_s , the system can attain its targets, such as efficiency, voltage gain, and ZVS, with lower dependence on f_s .

When utilizing a coupler for power transmission, it can also behave like an antenna, leading to potential radiation issues. Applying spread spectrum in IPT systems has proven to be an effective way to reduce both interference and radiation emanating from the coupler [11]. A typical example of triangular modulation is illustrated in Fig. 2, characterized by modulation frequency f_M . This setup broadens the fixed original frequency f_s to a range from f_L to f_H , with f_C serving as the central frequency. When frequency modulation is implemented in a conventional system, achieving ZVS and ZVDS at f_C , it impacts the transistor voltage v_{ds} , as shown in Fig. 2. Operating at $f_s = f_C$ enables the inverter to function optimally with ZVS and ZVDS. However, modulation of f_s to either f_L or f_H results in significant deviations from the desired operational

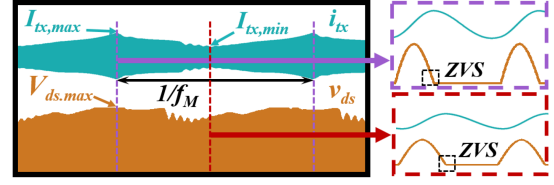


Fig. 3. Coil current and switch voltage under frequency modulation.

parameters, ultimately exacerbating EMI issues due to distorted v_{ds} , as shown in the bottom of Fig. 2. Consequently, frequency modulation is rarely employed in resonant inverters with high sensitivity to such deviations. In this article, $f_L = 0.95$ MHz, $f_H = 1.05$ MHz, $f_C = 1$ MHz, and $f_M = 2$ kHz. It is important to note that the choice of f_M is related to the requirements of the EMI receiver. Operating frequency range Δf , equals to $(f_H - f_L)/2$, directly influences the ZVS achievement and design candidates. It means a larger Δf would require the target system operates in a wider frequency range and narrow down the design range. The spectrum suppression A_{dB} would be mathematically predicted by the model as follows [12]:

$$A_{dB} = 10 \log_{10} \left(\frac{\Delta f}{f_M} \right). \quad (2)$$

B. Releasing Design Freedom

When applying spread spectrum techniques, the performance limitations of a class E inverter often stem from the stringent resonance requirements, which are highly sensitive to frequency and load variations. Unlike traditional methods that prioritize achieving perfect ZVS and ZVDS, this article proposes a novel approach that relaxes these requirements. By optimizing key design parameters, such as C_1 and C_2 , it is possible to achieve a more balanced tradeoff between efficiency, voltage stress, and load independence [10]. Building on this idea, this work seeks to advance the design of IPT systems, focusing on reducing electromagnetic radiation while maintaining high efficiency.

An exemplary IPT system utilizing the parameters depicted in Fig. 1 is selected for detailed analysis. The design variables C_1 and C_2 remain the focus, with C_3 resonating fully with L_{rx} at f_C . It would evaluate the design freedom of TX side, and C_3 could also be released from the RX perspective. In this investigation, the article gives up ZVDS while maintaining ZVS within the frequency range $f_s \in [f_L, f_H]$. For instance, by parameter sweeping, such as $C_1 \in [0 \text{ nF}, 1.6 \text{ nF}]$ and $C_2 \in [1 \text{ nF}, 4 \text{ nF}]$, additional design points can be identified through an ADS-based simulation. A successful design point, characterized by specific values of C_1 ($=1.3 \text{ nF}$) and C_2 ($=1.2 \text{ nF}$), is demonstrated in Fig. 3. Frequency modulation not only impacts the transistor's switching condition within each period as shown in the right figures, but also influences the system's overall performance over an extended time range. To achieve ZVS, v_{ds} should be zero during turn-ON instances within each modulation period, $1/f_M$. In addition, both the current and voltage will exhibit temporal variations during the modulation period.

In Fig. 3, the maximum and minimum magnitudes of the current, denoted as $I_{tx,max}$ and $I_{tx,min}$ respectively, allow to calculate

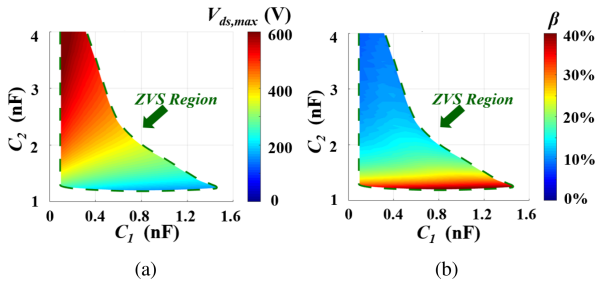


Fig. 4. Potential design points when ensuring ZVS. (a) $V_{ds,max}$. (b) β .

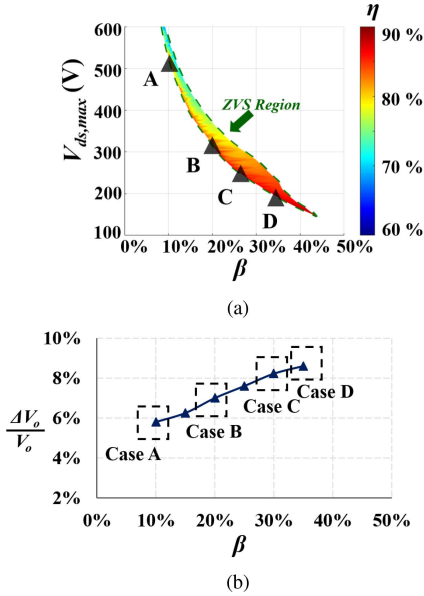


Fig. 5. Steady-state performance at different β . (a) Switch voltage and efficiency. (b) Output voltage ripple.

the current fluctuation ratio, represented as

$$\beta = \frac{I_{tx,max} - I_{tx,min}}{I_{tx,max} + I_{tx,min}}. \quad (3)$$

In addition, the switch voltage, affected by frequency perturbations, is defined by its peak value, denoted as $V_{ds,max}$. These parameters, $V_{ds,max}$ and β , are derived from simulations, as depicted in Fig. 4. It is crucial to highlight that all design scenarios are evaluated under consistent power levels and load conditions. The data points within the green zone indicate cases where ZVS operation is successfully achieved. Notably, when C_1 is kept constant, an increase in C_2 results in a higher $V_{ds,max}$ and a reduced β .

C. Tradeoff Design

The recorded state variables presented in Fig. 4 are not convenient for the final selection. Hence, it establishes a correlation between $V_{ds,max}$ and β in Fig. 5(a). For a given value of β , it is preferable to have the lowest possible $V_{ds,max}$ that falls within the ZVS boundary. In addition, the simulated efficiency η is represented within this ZVS region. It is observed that η is almost maximized at the bottom area. As a result, points along

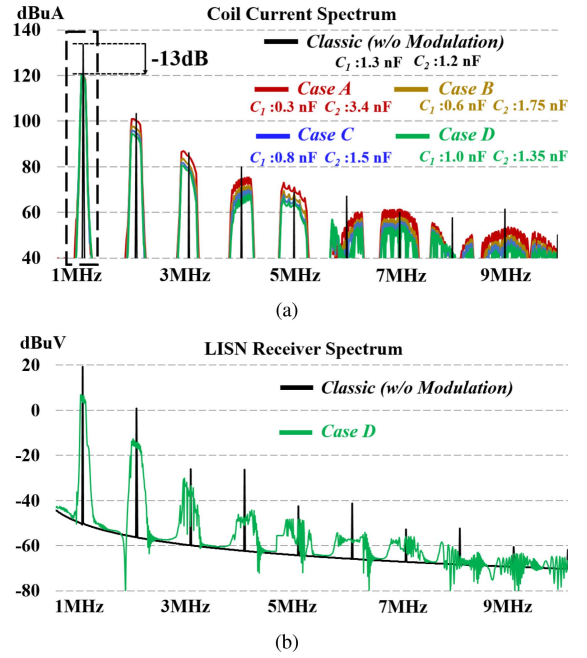


Fig. 6. Current spectrum in simulation. (a) Coil currents. (b) Conductive EMI measured by LISN.

the bottom boundary, such as cases A, B, C, and D, should be selected for further comparison. In the system, the induced voltage at RX is directly proportional to i_{tx} . Any nonzero value of β introduces output voltage ripple during the modulation period. Consequently, the system's output voltage ripple increases with larger values of β , as depicted in Fig. 5(b). A practical system would select C_f according to the ripple requirement. In this article, the load resistance R is set to 50Ω , and the filtering capacitor C_f is $50 \mu\text{F}$. Here, a constant C_f is kept for all the systems to ensure fair comparison. The increased β constitutes a significant drawback associated with the spread spectrum technique.

The effects of EMI reduction are demonstrated by analyzing the spectrum of the TX coil current. Fig. 6(a) examines all cases A–D under frequency modulation alongside a classical design without frequency modulation. In a classical 1-MHz system, the frequency components are highly concentrated, whereas, in all four cases with frequency modulation, the frequency components are more dispersed. This dispersion results in a 13-dB suppression of the current magnitude at 1 MHz, which is consistent across all cases due to the same power level and nearly identical RMS TX current. This outcome confirms the effectiveness of spread spectrum techniques. It should be noted that the current spectrum around 1 MHz would all contribute to the power transfer, and the proposed method would actually spread the originally concentrated power spectrum to a broader area with the same average power. In addition, similar reductions are observed in harmonic currents. Considering factors such as $V_{ds,max}$, efficiency η , output voltage V_{out} , and EMI reduction, case D emerges as the recommended design. The spread spectrum technique is effective in diminishing both conductive and radiative EMI, regardless of the converter topology. To

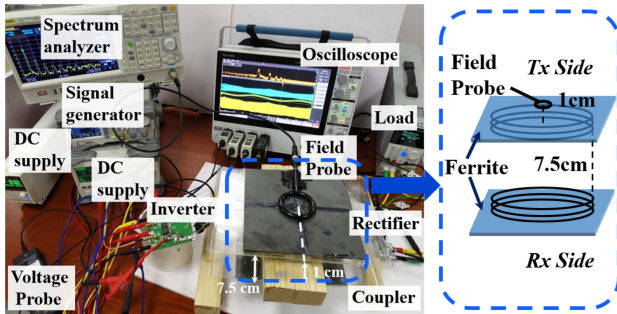


Fig. 7. Experiment setup.

 TABLE I
 DESIGN PARAMETERS

L_{tx}	L_{rx}	k	L_f	C_f	R_L
25.26 μH	25.71 μH	0.12	220 μH	50 μF	50 Ω
	Classical	Case A	Case B	Case C	Case D
C_1	1.3 nF	0.3 nF	0.6 nF	0.8 nF	1.0 nF
C_2	1.2 nF	3.4 nF	1.75 nF	1.5 nF	1.35 nF
C_3	1.0 nF	1.0 nF	1.0 nF	1.0 nF	1.0 nF
f	1 MHz	0.95–1.05 MHz			

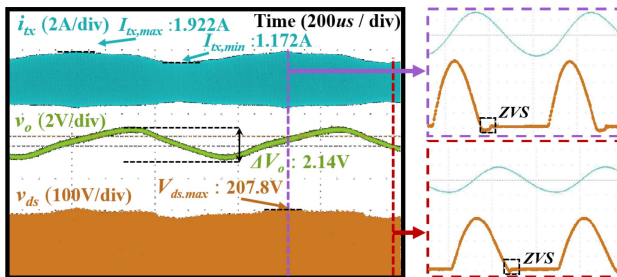


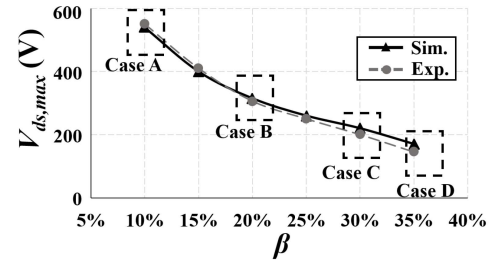
Fig. 8. Measured waveform under frequency modulation.

demonstrate this effect, the conductive EMI is compared as illustrated in Fig. 6(b).

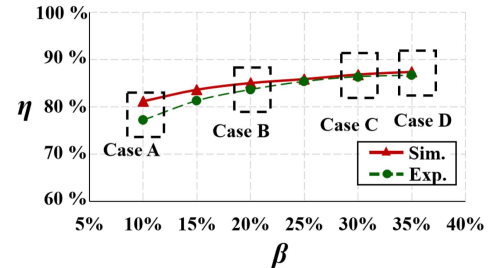
III. EXPERIMENT

To validate the design of spreading spectrum in an IPT system, an experimental setup, as Fig. 7, is implemented. The coupler structure and position are also shown in Fig. 7. This setup includes all the components outlined in Fig. 1 with the same circuit parameters. The parameters for different cases and the classical one are given in Fig. 6 and Table I. The output voltage of all cases in experiment is 25 V, and the output power is 12.5 W. To ensure accurate measurements, a high bandwidth current probe and a magnetic field probe are utilized. The magnetic field probe is positioned along the center axis of the coupler, with a distance of 1 cm from the TX coil. A magnetic layer is added to both side of the coupler and the shielding layer is not used. Such a setup would help to justify the EMI reduction effect which is induced by i_{tx} instead of i_{rx} .

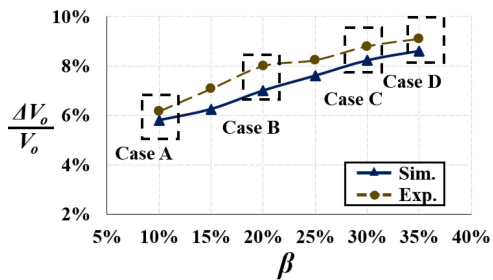
In order to evaluate the system, designated as case D, key variables, such as i_{tx} , v_o , and v_{ds} are measured and used to plot Fig. 8. The results illustrate that the implementation of spreading



(a)



(b)



(c)

 Fig. 9. Case comparison. (a) $V_{ds,max}$. (b) η . (c) $\frac{\Delta V_o}{V_o}$.

 TABLE II
 PARAMETERS COMPARISON

	Classical	Case A	Case B	Case C	Case D
EMI reduction	/	First harmonic - 13 dB			
V_{in}	36 V	93 V	60 V	42 V	30 V
$\frac{\Delta V_o}{V_o}$	/	6.17%	8.00%	8.80%	9.10%
η_{sim}	88.92%	81.17%	85.02%	86.82%	87.38%
η_{exp}	88.60%	77.23%	83.66%	86.36%	86.65%

spectrum techniques introduces current fluctuations and leads to an increased voltage ripple. Nevertheless, when the switching frequency f_s is varied within the range of $[f_L, f_H]$, an in-depth analysis of several switching cycles clearly demonstrates the achievement of ZVS operation.

Design points have been chosen along the lower boundary line of the ZVS region in Fig. 5(a), labeled as cases A–D. These points correspond to different values of β . To investigate the relationship between $V_{ds,max}$, η , ΔV_o , and β , both simulation and experimental results are presented in Fig. 9. Based on the evaluation of these metrics, case D is determined to be the most suitable option due to its low $V_{ds,max}$ and relatively high η , despite the sacrifice in output ripple. The parameters for different cases are compared as shown in Table II.

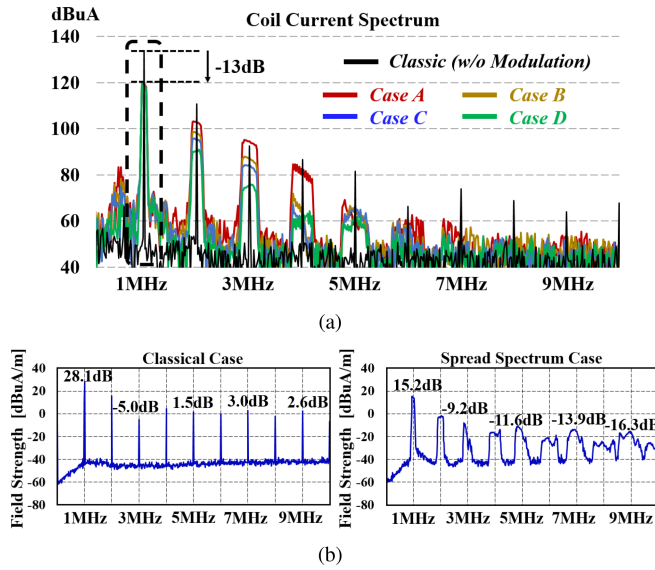


Fig. 10. Attenuation effects. (a) Coil current spectrum. (b) Field spectrum.

The current spectra of cases A–D are compared to a classical design, as shown in Fig. 10(a). These cases exhibit a 13-dB attenuation effect at the fundamental frequency, which is consistent with the simulation results. Similar attenuation effects are also observed at lower-order harmonics. The discrepancy between Figs. 10(a) and 6 above 7 MHz can be attributed to the limitations of the system model. It is important to note that circuit simulations may have difficulty predicting the high-frequency characteristics accurately. In addition, the magnetic field spectra of case D and the classical design are compared in Fig. 10(b). Notably, the field strength is reduced by 13 dB at 1 MHz, and similar EMI reduction effects are observed for other harmonic frequencies.

IV. CONCLUSION

This article introduces a customized IPT system specifically designed for spread spectrum technology. By loosening the design constraints on the resonant system, multiple objectives can be achieved simultaneously. Utilizing the proposed design

approach, the system ensures ZVS even under frequency modulation. As a result, a clear tradeoff can be achieved, encompassing high efficiency, low transistor voltage stress, low voltage ripple, and low EMI. Experimental results demonstrate a 13-dB reduction in the measured field compared to a classical design.

REFERENCES

- [1] H. Li and M. Fu, "Evaluation and suppression of high-frequency radiated EMI in inductive power transfer system," *IEEE Trans. Power Electron.*, vol. 39, no. 7, pp. 8998–9006, Jul. 2024.
- [2] H. Kim et al., "Coil design and measurements of automotive magnetic resonant wireless charging system for high-efficiency and low magnetic field leakage," *IEEE Trans. Microw. Theory Techn.*, vol. 64, no. 2, pp. 383–400, Feb. 2016.
- [3] T. Campi, S. Cruciani, F. Maradei, and M. Feliziani, "Magnetic field mitigation by multicoil active shielding in electric vehicles equipped with wireless power charging system," *IEEE Trans. Electromagn. Compat.*, vol. 62, no. 4, pp. 1398–1405, Aug. 2020.
- [4] Y. Li, K. Xie, Y. Ying, and Z. Li, "An improved hybrid shielding with LC coil for wireless power transfer system," *IEEE Trans. Electromagn. Compat.*, vol. 60, no. 3, pp. 720–731, Jun. 2018.
- [5] S. Alshhawy, A. Barakat, and R. K. Pokharel, "Efficient and low leakage WPT system with integrated uncomplicated matching circuit rectifier using metamaterial director and isolator for biomedical application," *IEEE J. Electromagn., RF, Microw. Med. Biol.*, vol. 8, no. 2, pp. 144–154, Jun. 2024.
- [6] F. Pareschi, R. Rovatti, and G. Setti, "EMI reduction via spread spectrum in DC/DC converters: State of the art, optimization, and tradeoffs," *IEEE Access*, vol. 3, pp. 2857–2874, 2015.
- [7] S. A. Chowdhury, S.-W. Kim, S.-M. Kim, J. Moon, I.-K. Cho, and D. Ahn, "Automatic tuning receiver for improved efficiency and EMI suppression in spread-spectrum wireless power transfer," *IEEE Trans. Ind. Electron.*, vol. 70, no. 1, pp. 352–363, Jan. 2023.
- [8] S. A. Chowdhury, S. Kim, S. Kim, J. Moon, I. Cho, and D. Ahn, "Reducing/increasing tuning capacitor for frequency-modulated spread-spectrum inductive power transfer," *IEEE Trans. Power Electron.*, vol. 38, no. 11, pp. 13384–13395, Nov. 2023.
- [9] S. A. Chowdhury, S. Kim, S. Kim, I. Cho, and D. Ahn, "Resonant tuning rectifier for parallel compensated receivers in wireless power transfer," *IEEE Trans. Ind. Electron.*, early access, 2024, doi: [10.1109/TIE.2024.3390737](https://doi.org/10.1109/TIE.2024.3390737).
- [10] Y. Jiang, J. Liang, H. Wang, Y. Liu, and M. Fu, "Load-impedance-insensitive design of high-efficiency class EF inverters," *IEEE Trans. Power Electron.*, vol. 39, no. 2, pp. 1958–1962, Feb. 2024.
- [11] K. Inoue, K. Kusaka, and J.-I. Itoh, "Reduction in radiation noise level for inductive power transfer systems using spread spectrum techniques," *IEEE Trans. Power Electron.*, vol. 33, no. 4, pp. 3076–3085, Apr. 2018.
- [12] J. Kim, D. G. Kam, P. J. Jun, and J. Kim, "Spread spectrum clock generator with delay cell array to reduce electromagnetic interference," *IEEE Trans. Electromagn. Compat.*, vol. 47, no. 4, pp. 908–920, Nov. 2005.